PCCP

PAPER

View Article Online
View Journal | View Issue

Cite this: *Phys. Chem. Chem. Phys.*, 2014, **16**, 4843

$ZnFe_2O_4$ nanoparticles dispersed in a highly porous silica aerogel matrix: a magnetic study†

S. Bullita,[a] A. Casu,[b] M. F. Casula,[a] G. Concas,[c] F. Congiu,[c] A. Corrias,*[ad] A. Falqui,[ab] D. Loche[a] and C. Marras[a]

Received 10th October 2013,
Accepted 14th January 2014

DOI: 10.1039/c3cp54291b

www.rsc.org/pccp

We report the detailed structural characterization and magnetic investigation of nanocrystalline zinc ferrite nanoparticles supported on a silica aerogel porous matrix which differ in size (in the range 4–11 nm) and the inversion degree (from 0.4 to 0.2) as compared to bulk zinc ferrite which has a normal spinel structure. The samples were investigated by zero-field-cooling–field-cooling, thermo-remnant DC magnetization measurements, AC magnetization investigation and Mössbauer spectroscopy. The nanocomposites are superparamagnetic at room temperature; the temperature of the superparamagnetic transition in the samples decreases with the particle size and therefore it is mainly determined by the inversion degree rather than by the particle size, which would give an opposite effect on the blocking temperature. The contribution of particle interaction to the magnetic behavior of the nanocomposites decreases significantly in the sample with the largest particle size. The values of the anisotropy constant give evidence that the anisotropy constant decreases upon increasing the particle size of the samples. All these results clearly indicate that, even when dispersed with low concentration in a non-magnetic and highly porous and insulating matrix, the zinc ferrite nanoparticles show a magnetic behavior similar to that displayed when they are unsupported or dispersed in a similar but denser matrix, and with higher loading. The effective anisotropy measured for our samples appears to be systematically higher than that measured for supported zinc ferrite nanoparticles of similar size, indicating that this effect probably occurs as a consequence of the high inversion degree.

1. Introduction

Transition metal spinel ferrites MFe_2O_4 (M being a bivalent transition metal cation) are of great interest for their remarkable magnetic, catalytic, optical and electrical properties, which strongly depend on their structure. The spinel structure, belonging to space group *Fd3m*, is characterized by a cubic unit cell containing 8 MFe_2O_4 formula units with a cubic close packing of 32 oxygen anions, where the 24 cations are located in 8 of the 64 tetrahedral sites (A sites) and in 16 of the 32 octahedral sites (B sites).[1]

Nanoparticles of spinel ferrites find applications in magnetic storage systems,[2] site-specific drug delivery,[3] magnetic resonance imaging[4] and as photomagnetic materials,[5] due to their interesting magnetic and catalytic properties, frequently different from those of bulk materials.[6] The magnetic properties of ferrite nanoparticles depend on both the size of the nanoparticles and the cation distribution in the spinel structure.

Zinc ferrite is a very good choice to study these effects because zinc is a non-magnetic atom and therefore the magnetic properties only depend on the distribution of the iron cations. Bulk zinc ferrite, a normal spinel with Zn^{2+} cations occupying tetrahedral sites and Fe^{3+} cations occupying octahedral sites, is not magnetic at room temperature, and becomes antiferromagnetic below $T_{Néel}$ = 10 K.[7] Instead, it has been reported a rearrangement of the cation distribution when this ferrite is at the nanoscale, with the formation of a partially inverted structure responsible for an enhanced magnetization.[8–12]

Most of the studies on zinc ferrite nanoparticles have been carried out on unsupported nanoparticles,[8–17] or on nanoparticles supported on silica xerogel with a high loading of zinc ferrite.[14] To date, the only work on zinc ferrite nanoparticles within a highly porous matrix has been our recent study by X-ray absorption spectroscopy of the variation of the inversion degree during the growth of zinc ferrite nanoparticles within a highly porous aerogel silica matrix, which keeps the nanoparticles

[a] *Dipartimento di Scienze Chimiche e Geologiche, Università di Cagliari, and INSTM, S.P. Monserrato-Sestu km 0.700, 09042 Monserrato, CA, Italy*
[b] *Nanochemistry, Istituto Italiano di Tecnologia, I.I.T. Via Morego 30, 16163 Genova, Italy*
[c] *Dipartimento di Fisica, Università di Cagliari, and INSTM, S.P. Monserrato-Sestu km 0.700, 09042 Monserrato, CA, Italy*
[d] *School of Physical Sciences, Ingram Building,, University of Kent, Canterbury, CT2 7NH, UK. E-mail: a.corrias@kent.ac.uk*

† Electronic supplementary information (ESI) available. See DOI: 10.1039/c3cp54291b

wide apart.[18] This study has shown that the degree of inversion decreases as the zinc ferrite nanoparticles grow, as already observed in both unsupported and supported nanoparticles.[14,15] In particular, the reported value of the inversion degree in ref. 14 (0.126) is smaller than the values found for our aerogel samples;[18] however in ref. 14 the degree of inversion was only measured for the biggest particles with a mean size of about 20 nm.

The magnetic properties of zinc ferrite have been investigated in the literature on unsupported nanoparticles and also on nanocomposites made out of a high loading of nanoparticles dispersed in a silica matrix, by means of static magnetization measurements and Mössbauer spectroscopy for a large range of particle sizes.[14–16] In particular, similar values of static magnetization and Mössbauer blocking temperature were determined for samples with very different particle sizes. These findings were explained on the basis of a variation of the effective anisotropy constant, which decreases upon increasing the particle volume due to the decrease of the surface contribution and the magneto-crystalline anisotropy, which is supposed to decrease when the inversion parameter decreases.[14,15]

To date, the magnetic properties of zinc ferrite nanoparticles dispersed in a highly porous matrix, which keeps them apart, have not been studied. In particular, since our previous studies by X-ray absorption spectroscopy have allowed us to determine the variation of the inversion degree as the zinc ferrite nanoparticles grow inside a highly porous silica aerogel matrix, in this work we investigate the dependence of the magnetic properties of the nanoparticles on their inversion degree. The textural and structural properties are thoroughly assessed by means of X-ray diffraction, Transmission Electron Microscopy and N_2 physisorption at 77 K. The blocking temperatures and the effective anisotropy constant are determined by means of static and dynamic magnetization measurements and Mössbauer spectroscopy, leading also to an evaluation of contribution of the inter-particle interactions to the collective magnetic behaviour. The evolution of the saturation magnetization and the coercive field with the inversion degree are evaluated by the measurement of the hysteresis loops.

2. Experimental section

The nanocomposite samples were prepared using a synthetic approach developed in our laboratories for $CoFe_2O_4$–SiO_2 and successfully extended to several other nanocomposites,[19,20] which makes use of tetraethoxysilane ($Si(OC_2H_5)_4$, Aldrich, 98%, TEOS) as a silica precursor, iron(III) and zinc(II) nitrates ($Fe(NO_3)_3{\cdot}9H_2O$ and $Zn(NO_3)_2{\cdot}6H_2O$, Aldrich, 98%) as precursors for the ferrite phase, and absolute ethanol (EtOH, Fluka) as mutual solvent. The precursors were added in such a way to obtain a final nanocomposite containing a nominal ratio of 10 wt% $ZnFe_2O_4/(ZnFe_2O_4 + SiO_2)$. The ethanolic solution of the metal salts was added into the pre-hydrolyzed TEOS under acidic catalysis. A hydro-alcoholic solution of urea (NH_2CONH_2, Aldrich, >99.0%) was then added under reflux for 2 hours at 85 °C as a basic gelation agent. Gelation of the sols occurred after less than 2 days in closed vials at 40 °C. The alcogel was submitted to high temperature supercritical drying in an autoclave (Parr, 300 cm^3) according to the procedure summarized as follows. The alcogel was inserted into the autoclave filled with 70 mL of ethanol and flushed with N_2 before taking the solvent to the supercritical state by heating the autoclave up to 330 °C when the pressure reaches 70 atm. The autoclave was then vented and a highly porous aerogel sample was obtained. The sample was thermally treated in static air at different temperatures and times: 450 °C for 1 h (sample named ZF450_1), 750 °C for 1 h (ZF750_1), 750 °C for 6 h (ZF750_6) and 900 °C for 1 h (ZF900_1).

Wide-angle X-Ray Diffraction (XRD) patterns were recorded on a Panalytical Empyrean diffractometer equipped with a graphite monochromator on the diffracted beam and an X'Celerator linear detector. The scans were collected within the range of 10–90° (2θ) using Cu Kα radiation. The average crystallite size was calculated by applying the Scherrer formula, from the peak full width at half maximum (FWHM) corrected for instrumental broadening determined on a standard LaB_6 sample.

Transmission electron microscopy (TEM) images were recorded on a Hitachi H-7000 instrument running at 100 kV. Prior to observation, the samples were finely ground and deposited on a carbon-coated copper grid.

Surface areas, pore sizes and pore volumes were obtained from N_2 adsorption–desorption measurements at 77 K recorded on a Sorptomatic 1990 System (Fisons Instrument). Surface area was estimated using the Brunauer–Emmett–Teller (BET) model,[21–23] pore size and pore volumes were estimated using the Barret–Joyner–Halenda (BJH) method.[24]

The Mössbauer absorption spectra were obtained at 77 K and at room temperature (RT) in standard transmission geometry, using a source of ^{57}Co in rhodium with activity of 370 MBq. The calibration was performed using a 6 μm thick natural α-Fe foil; the measured full width at half maximum of the absorption peak is 0.29 ± 0.1 mm s^{-1}. The isomer shift values were referred to α-Fe. The measurements were carried out on powder samples contained in a copper/Plexiglas holder (at 77 K) and in a Plexiglas holder (at RT). The surface density of the absorbers was 90 mg cm^{-2} of the sample; the measurements were performed with an amount of iron in the samples corresponding to an effective thickness $t \sim 1.7$ in order to avoid an excessive peak broadening.

The analysis of Mössbauer spectra was performed by fitting the data by peaks of Lorentzian shape and applying a least squares method. The spectra were analysed using two components, a two peak component and a six peak one. The two peak component is associated with the superparamagnetic fraction; the six peak component corresponds to the absorption split by the magnetic field and is associated with the magnetically blocked fraction of the sample. The ratio of the areas of the components gives the relative amount of the superparamagnetic and blocked fractions of a sample at a given temperature.

Measurements of static and dynamic (ac) magnetizations and hysteretic behavior of the samples were performed on a Quantum Design MPMS SQUID magnetometer, equipped with

a superconducting magnet producing fields up to 70 kOe. Zero-field-cooled (ZFC) magnetizations were measured by cooling samples in the zero magnetic field and then by increasing the temperature in an applied field of 25 Oe, while field-cooled (FC) curves were recorded by cooling the samples in the same field of 25 Oe. The ac magnetizations were measured in an oscillating field of 5 Oe, in the frequency range 0.1–1000 Hz. The field dependence of the magnetization (hysteresis loop) was recorded up to 70 kOe, at $T = 5$ K. Finally, thermoremanent magnetization (TRM) was measured in the zero field while heating the samples, after cooling them down in a field of 25 Oe.

3. Results and discussion

3.1 XRD, TEM and N_2 physisorption

Fig. 1 shows the XRD patterns of the nanocomposite submitted to different thermal treatments. At low calcination temperatures (sample ZF450_1) only the halo at $2\theta \approx 20^\circ$ due to the amorphous SiO_2 matrix can be clearly observed, together with some very weak peaks (at $2\theta \approx 36$ and 63°) which cannot be identified unambiguously. It seems likely that Fe is present in the form of ferrihydrite [PDF-2 Card no. 29-712], a poorly crystalline iron(III) oxide hydroxide, on the basis of the pattern of samples synthesized with double amounts of the nanoparticle precursors, reported in the ESI† (Fig. SI_1). Zinc is likely present in an amorphous phase, as inferred from the pattern of a sample prepared using only the zinc precursor and leaving out the iron precursor in the synthesis (Fig. SI_2, ESI†), which does not show any peak.

Peaks due to the formation of the Zn ferrite phase [PDF-2 Card no. 22-1012] superimposed to the amorphous silica halo appear after treatment at 750 °C and become more evident and sharper in the series ZF750_1, ZF750_6, ZF900_1. The average crystallite dimensions of the ferrite nanoparticles, as derived from the peak FWHM, are 4.2 nm, 6.8 nm and 11.1 nm, for the ZF750_1, ZF750_6 and ZF900_1 samples, respectively. All these results point out that the zinc ferrite nanoparticles form as a consequence of the reaction between the two precursors present after calcination at 450 °C, *i.e.* the amorphous zinc containing phase and the poorly crystalline iron phase. The evolution of the XRD patterns with the time and temperature of the thermal treatment is consistent with an increasing amount of precursors being progressively converted in the partially inverted zinc ferrite nanophase, while at the same time the inversion degree decreases with the thermal treatments.[18]

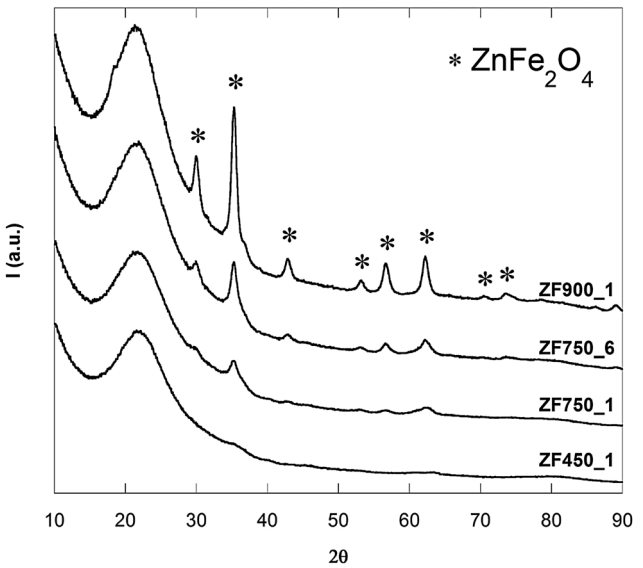

Fig. 1 XRD patterns of the $ZnFe_2O_4$–SiO_2 nanocomposite aerogel submitted to different thermal treatments.

Representative TEM bright field (BF) and dark field (DF) images of the aerogel nanocomposites after different thermal treatments are reported in Fig. 2. The TEM BF images clearly show the highly branched silica network of the nanocomposites, and the porous open structure typical of aerogels, with *meso-* and macropores. The DF images show the presence of nanocrystals homogeneously dispersed throughout the silica matrix as a result of the mixing of the dispersed and matrix phase precursors at the early stages of the sol–gel procedure and of the controlled gelation. Statistical analysis of the TEM images indicates that the nanocrystal size increases with the calcination conditions from 4.0 nm, to 8.3 nm and 10.2 nm, with a standard deviation which is 1.5 nm for the three distributions, in good agreement with the XRD data.

Fig. 3 shows the isotherm of the $ZnFe_2O_4$–SiO_2 aerogel after calcination at the highest temperature, *i.e.* the ZF900_1 nanocomposite. The isotherm is of type IV with an H1 hysteresis lying at high relative pressures, indicating the occurrence of interconnected mesopores with large size typical of the aerogel structure. In particular, the pore size is in the range 23–40 nm, the pore volume is 2.97 $cm^3\ g^{-1}$ and the surface area is 282 $m^2\ g^{-1}$. These values are comparable to those obtained for aerogel nanocomposites containing cobalt, nickel or manganese ferrite nanoparticles synthesized using a similar procedure.[20] Similar results were obtained for the ZF750_6 sample (not shown here).

3.2 Mössbauer spectroscopy and magnetic measurements

Further characterization by Mössbauer spectroscopy and magnetic measurements was carried out on the samples where the presence of zinc ferrite nanoparticles was evidenced by XRD and TEM, *i.e.* ZF750_1, ZF750_6 and ZF900_1.

None of the Mössbauer spectra of the ZF750_1, ZF750_6 and ZF900_1 samples showed a magnetically ordered blocked fraction at RT: therefore the spectra of the same samples were also collected at 77 K. Fig. 4 shows the spectrum of the ZF750_1 sample at 77 K, which shows a six-peak structure, associated with a magnetically ordered blocked fraction of the sample, along with a two-peak structure associated with a superparamagnetic fraction.[25] The spectrum has been fitted using one sextet for the blocked fraction and one doublet for the superparamagnetic fraction and the results of the fit for the two fractions are given in Table 1. At 77 K the sample is blocked for about half volume; the blocked fraction amounts to 53%. In this spectrum the fit gives an average value of the distribution of hyperfine magnetic fields (HMF) of the nanoparticles,

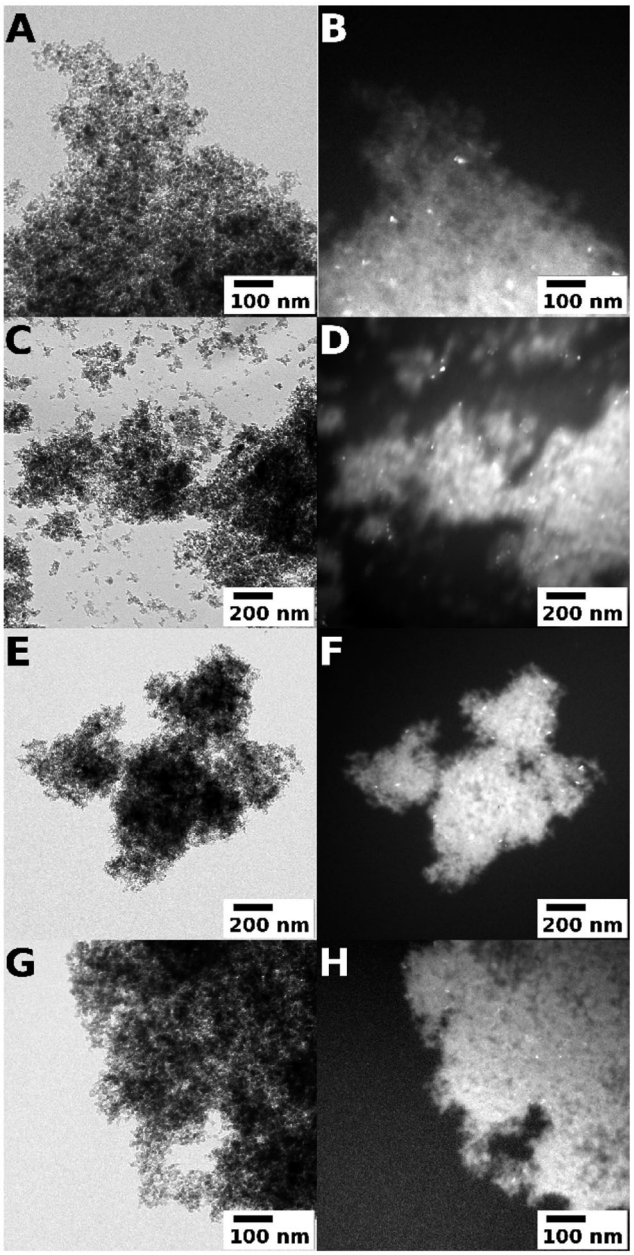

Fig. 2 TEM BF and DF images of (A, B) ZF900_1, (C, D) ZF750_6, (E, F) ZF750_1 and (G, H) ZF450_1.

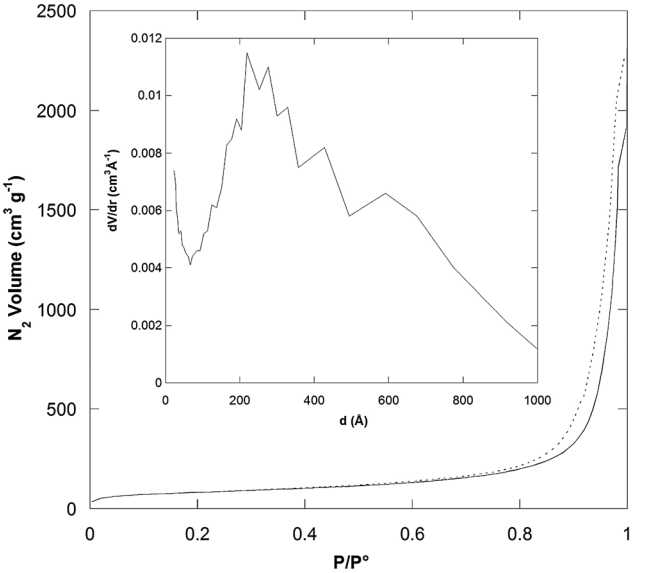

Fig. 3 N_2 physisorption isotherms at 77 K, and corresponding BJH pore size distribution as derived from the desorption branch (inset), for the ZF900_1 aerogel nanocomposite.

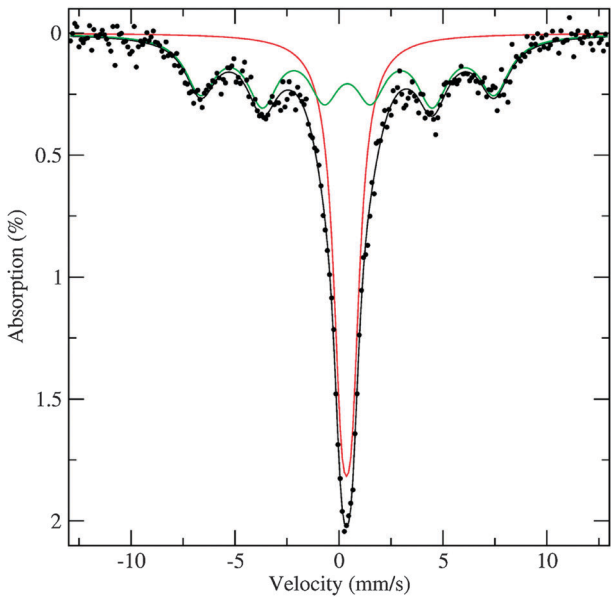

Fig. 4 Mössbauer spectrum of the sample ZF750_1 at 77 K. The experimental points are reported as dots. The fitting curve is shown as a black line; the blocked and superparamagnetic components are shown as green and red lines respectively.

because the blocked fraction did not complete the transition from the superparamagnetic to the blocked state which explains the largely reduced value, compared to the HMF of the bulk.[15] The spectrum of the ZF750_6 sample at 77 K is plotted in Fig. 5 and it shows the magnetically ordered blocked fraction of the sample along with the superparamagnetic fraction. The blocked fraction of the sample at 77 K is only slightly smaller than the fraction of the ZF750_1 sample, amounting exactly at 48%. Finally, the spectrum of the ZF900_1 sample at the same temperature, which is given in Fig. 6, has also been fitted with the same two components, but in this case the blocked fraction is much smaller (16%). The results of the fits of the three spectra are compared in Table 1.

It should be pointed out that the three spectra have all been fitted using components due to trivalent ions, as indicated by the values of isomer shift and quadrupole splitting;[25] no trace of divalent irons has been detected. When the areas of the blocked and superparamagnetic components are equal, the sample stays at the blocking temperature (T_{bM}) as defined for Mössbauer spectroscopy, which has a measuring time of 5×10^{-9} s. The Mössbauer blocking temperature was determined using the relative areas of the blocked and the superparamagnetic

Table 1 Mössbauer parameters of $ZnFe_2O_4$–SiO_2, as obtained by fitting the spectra at 77 K of the indicated samples. The values of isomer shift (δ), quadrupole splitting (Δ), hyperfine magnetic field (B) and relative intensity (A) of the components are given, along with the Mössbauer blocking temperature T_{bM}. Statistical errors are given in parentheses as errors in the last digit

Sample	δ (mm s^{-1})	Δ (mm s^{-1})	B (T)	A (%)	T_{bM} (K)
ZF750_1	0.47(1)	0.49(1)		47(1)	80(1)
	0.51(1)		44.1(5)	53(1)	
ZF750_6	0.46(1)	0.46(1)		52(1)	75(1)
	0.47(1)		43.7(5)	48(1)	
ZF900_1	0.46(1)	0.42(1)		84(1)	31(1)
	0.46(1)		46.4(5)	16(1)	

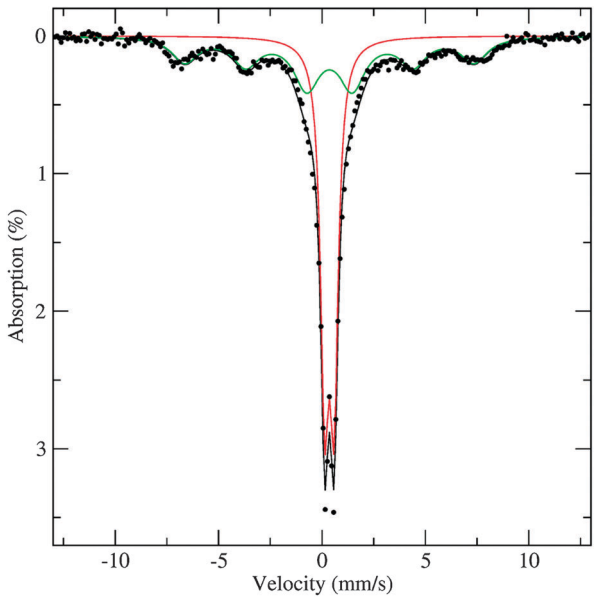

Fig. 5 Mössbauer spectrum of the sample ZF750_6 at 77 K. The experimental points are reported as dots. The fitting curve is shown as a black line; the blocked and superparamagnetic components are shown as green and red lines respectively.

components and the standard deviation of the particle volume distribution, as determined by TEM microscopy, in order to consider the evolution of the blocked and superparamagnetic fractions with the temperature.[26] Therefore the blocking temperature results 80 K for ZF750_1, 75 K for ZF750_6, and 31 for ZF900_1.

The magnetic properties of the ZF750_1, ZF750_6 and ZF900_1 samples were investigated by SQUID magnetometry, normalizing the results with respect to the total mass of the sample.

Fig. 7 shows the measurements of the magnetization *versus* temperature, according to the ZFC–FC procedure, for the ZF750_1, ZF750_6 and ZF900_1 samples. The ZFC–FC magnetization curves show a superparamagnetic behavior for all the systems.[27] The ZFC curve of the ZF750_1 sample displays a broad maximum in the range of 4–140 K, the latter temperature (T_{irr}) being the one at which the ZFC and FC curves superimpose. In particular, the temperature corresponding to the maximum of

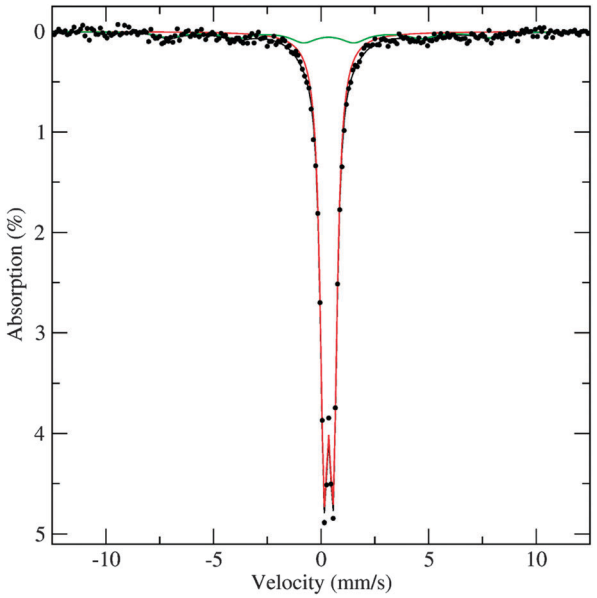

Fig. 6 Mössbauer spectrum of the sample ZF900_1 at 77 K. The experimental points are reported as dots. The fitting curve is shown as a black line; the blocked and superparamagnetic components are shown as green and red lines respectively.

the ZFC curve, T_{max}, which is related in a complex way to the effective anisotropy energy barrier, is 37 K. The ZFC curves of ZF750_6 and ZF900_1 also show a broad maximum in a similar thermal range, T_{max} being around 31 K for the ZF750_6 sample and 15 K for the ZF900_1 sample, while the corresponding T_{irr} are 112 and 175 K, respectively. The trend of the Mössbauer blocking temperatures, T_{bM}, for the three samples is therefore confirmed by the maximum temperature (T_{max}) of the magnetization curves, which measures the same blocking effect with the larger measuring time of the DC magnetometry, the latter being defined in the range 10–100 s.

The trend of both the Mössbauer blocking temperature (T_{bM}) and the maximum temperature (T_{max}) of the magnetization curves for the three samples is therefore not the one which is expected as a function of particle size, since larger nanoparticles should show larger blocking temperatures. Instead, the trend is exactly the opposite, if we take into account the particle sizes determined by both XRD and TEM.

This result points out that the evolution of the blocking temperature must be due to some other difference among the samples, which overwhelms the size effect. In fact, a XANES and EXAFS study carried out on the same samples has indicated that the three samples have a different inversion degree.[18] In particular all the three samples are partially inverted, differently from bulk zinc ferrite which is a normal spinel, and a higher degree of inversion is observed for ZF750_1, which progressively decreases, being 0.41, 0.29, and 0.21 for ZF750_1, ZF750_6 and ZF900_1 samples, respectively. This partial and different degree of inversion of the crystalline spinel structure between the samples is expected to have a critical effect on their magnetic behaviour.[9,14]

The observed effect of T_{max} decreasing with the increase of the duration and/or temperature of the thermal treatment

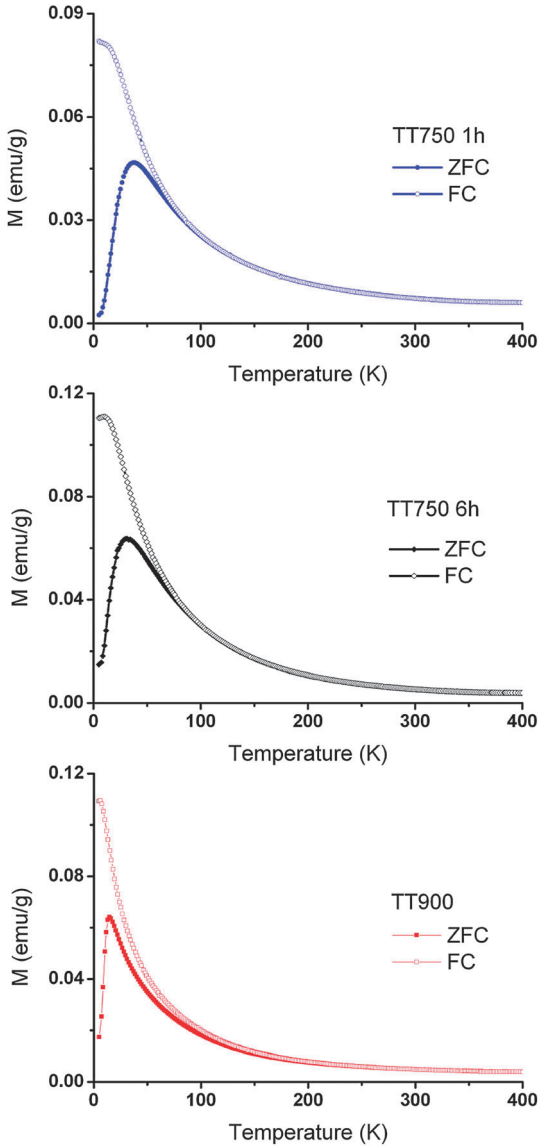

Fig. 7 ZFC–FC static magnetization curves, obtained using a magnetic field of 25 Oe, of ZF750_1, ZF750_6 and ZF900_1 samples.

could also be regarded in a different way. In fact, it could also be explained as an indirect effect of the cation reallocation in the ferrite spinel structure toward the normal spinel state. Such a reallocation could give rise to a decrease of the effective magnetic size inside the magnetically active particles, which would produce a decrease of T_{max}. However, this hypothesis cannot be verified easily, since this would require to know *a priori* the effective anisotropy constant of each sample or the saturation magnetization of the corresponding bulk phase. The anisotropy constant of partially inverted ferrite is not known, because it depends in an unknown way on the inversion degree. Moreover, the known saturation magnetization of the bulk phase corresponds to the antiferromagnetic and normal spinel phase, not directly comparable with any of our samples.

According to Neel theory,[28] the magnetic moment of non-interacting single domain identical particles, with uniaxial anisotropy, fluctuates between the two directions of easy axes with a relaxation time that follows an Arrhenius law:

$$\tau = \tau_0 \exp(E_b/k_B T) \quad (1)$$

where τ_0 is a pre-exponential factor and E_b the energy barrier; $E_b = K_A V$, where K_A is the effective anisotropy constant and V is the volume of the particle. Besides defining T_{Block} (blocking temperature)[29] as the temperature T for which the time τ is equal to the typical measurement time of each technique (τ_m), different values are obtained from Mössbauer spectroscopy and SQUID magnetometry. In particular, T_{Block} corresponds to T_{bM} in Mössbauer spectroscopy, while in SQUID magnetometry T_{Block} is usually taken equal to T_{max}.

The combined use of Mössbauer spectra and DC magnetization measurements provides a way to evaluate the average energy barrier $<E_b> = K_A<V>$. In particular, the Arrhenius-like law reported above as eqn (1), using the measured values of the blocking temperature (T_{bM} from Mössbauer and T_{max} from static magnetization), with the corresponding measuring time τ_m ($\tau_m = 5 \times 10^{-9}$ s and $\tau_m = 100$ s for Mössbauer and static magnetization, respectively), was used to evaluate the energy barrier $<E_b>$. By following this procedure $<E_b>$ results to be 2.3×10^{-13} erg, 1.7×10^{-13} erg and 9.5×10^{-14} erg for the ZF750_1, ZF750_6, ZF900_1 samples, respectively. The average energy barrier values were then used to evaluate K_A by considering spherical nanoparticles with the average sizes determined by XRD diffraction, obtaining $K_A = 5.8 \times 10^6$ erg cm^{-3}, 1.0×10^6 erg cm^{-3} and 1.3×10^5 erg cm^{-3} for the ZF750_1, ZF750_6 and ZF900_1 samples, respectively. These values of the energy barrier and the effective anisotropy constant are in the range expected for ferrimagnetic nanoparticles,[30] but higher than those reported in ref. 14 for zinc ferrite nanoparticles of similar size, dispersed with higher loading in an amorphous silica matrix.

Fig. 8 shows the hysteresis loops measured at 5 K for the ZF750_1, ZF750_6 and ZF900_1 samples, respectively, and Table 2 summarizes the parameters obtained from these measurements.

Considering the ferrimagnetic nature of the zinc ferrite nanoparticles contained in all the samples and due to the partial inversion of their spinel crystalline structure, the saturation magnetization (M_{sat}) was derived from a plot of M *versus* $1/H$, extrapolating the M values for $1/H \rightarrow 0$.[8,16] It should be noticed that all the samples are quite far from the saturation. This could be due to concomitant and different causes, the most likely being the presence of very small ferrite particles that are still relaxing even at low temperature and high fields and, as already reported also in the recent literature, the occurrence of a non-negligible surface spin canting in the ferrite nanoparticles.[31]

The data obtained from the hysteresis loops indicate first of all that saturation magnetization, M_S, increases with the increase of the temperature and length of the thermal treatment, *i.e.*, as first approximation, with the amount of Zinc ferrite nanophase contained in the samples, as inferred from the evolution of the XRD patterns with the time and temperature of the thermal treatment, and then with the related mean nanoparticle size of the sample; secondly, the corresponding decrease in H_c confirms

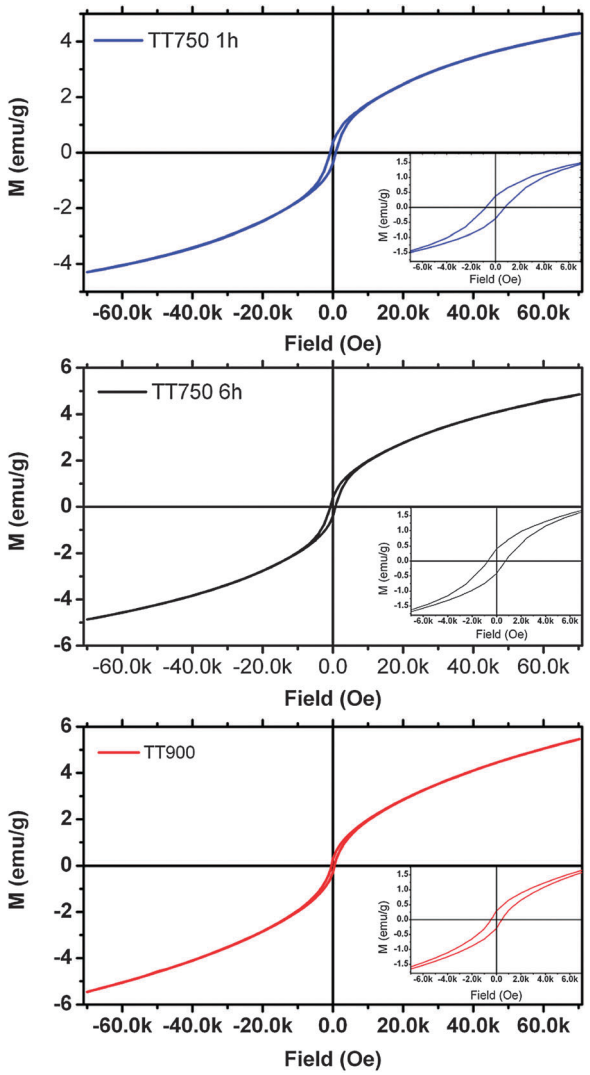

Fig. 8 Hysteresis loop obtained at T = 5 K of samples ZF750_1, ZF750_6 and ZF900_1.

Table 2 Parameters obtained by the hysteresis loops of the sample: H_c: coercive field; M(7 T): magnetization measured at 7 T; M_S: saturation magnetization extrapolated at a high field; M_r/M_S: reduced remnant magnetization

Sample	H_c (Oe)	M(7 T) (emu g^{-1})	M_S (emu g^{-1})	M_r/M_S
ZF750_1	786	4.3	6.3	0.06
ZF750_6	718	4.9	7.6	0.05
ZF900_1	444	5.5	9.2	0.03

the decrease of the anisotropy constant, in agreement with what already observed from the trend in the blocking temperature determined both from the ZFC maxima and Mössbauer spectroscopy; finally, the trend of the reduced remnant magnetization M_r/M_S is very similar to that reported in several papers on zinc ferrite nanoparticles.[7,32]

In addition to this, as already observed, the interpretation of the observed magnetic properties of the three samples should take into account both the increase of the amount of the zinc ferrite nanophase and the concomitant decrease of the inversion degree with particle size, going from the ZF750_1, to ZF750_6 and ZF900_1 sample, respectively. It is well known from the literature on zinc ferrite nanoparticles that changes in the inversion degree have a dramatic effect on the saturation magnetization of the material,[9,33] which has the tendency to increase when the inversion degree increases. On the other hand, it has never been reported in the literature how the two parameters are quantitatively correlated. Meanwhile, as reported above, in our samples an amorphous phase containing zinc, present in the sample calcined at 450 °C together with a poorly crystalline iron containing phase, is converted in zinc ferrite with the increase of the time and the temperature of the thermal treatment. These two results have an opposite effect on the saturation magnetization of the samples. The increase in the amount of ferrite gives rise to an increase of the saturation magnetization, while the concomitant decrease of the inversion degree gives rise to a decrease of the saturation magnetization. The observed behavior clearly indicates that the first effect is higher than the second one, since an overall increase of M_S with the thermal treatment was measured. Furthermore, it is very likely that the variation in the inversion degree has a big effect on the magnetocrystalline anisotropy of the material, giving an additional contribution to the two ones that are contributing in our case to the effective particle anisotropy: the magnetocrystalline contribution (which depends on the inversion degree) and the surface contribution, which decreases with the increase of nanoparticle size. All these points further help to recognize the overall critical effect of the different partial spinel inversion on both the single particle and collective magnetic behavior of our samples. For all these reasons, a quantitative interpretation of the trend observed for the parameters extracted from the hysteresis loops is not possible. Moreover, the amount of zinc ferrite present in each sample cannot be estimated by using the M_S values, since the saturation magnetization changes with the inversion degree, and it is therefore different to the value of bulk zinc ferrite, which is a normal spinel.

To obtain a better estimate of the effective anisotropy constant (K_A) of the three samples, dynamic (ac) ZFC measurements were performed on the three samples, using a magnetic field of 5 Oe oscillating from 0.1 to 100 Hz. The real (in phase) component, m', of the complex magnetization is reported in Fig. 9 for each samples and for all the frequencies of the oscillating field.

As clearly reported by Tronc *et al.*,[29] the maximum of each m' ac ZFC curves could be taken as the true value of the blocking temperature (T_{Block}) for the sample, where the corresponding τ_m, the measurement time of the magnetic measurement, is simply given by the reciprocal of the frequency of the oscillating field. Now, considering the logarithmic linearization of the well-known Arrhenius-like equation,[28] which describes the superparamagnetic oscillation of single domain particles, we obtain that

$$\ln \tau_m = \frac{K_A \cdot \langle V \rangle}{k_B} \cdot \frac{1}{T_B} + \ln \tau_0 \qquad (2)$$

where K_A is the effective anisotropy constant, $\langle V \rangle$ is the mean nanoparticle volume, k_B is the Boltzmann constant and τ_0 is the pre-exponential factor, expected in the range 10^{-9}–10^{-13} s for single domain nanoparticles.

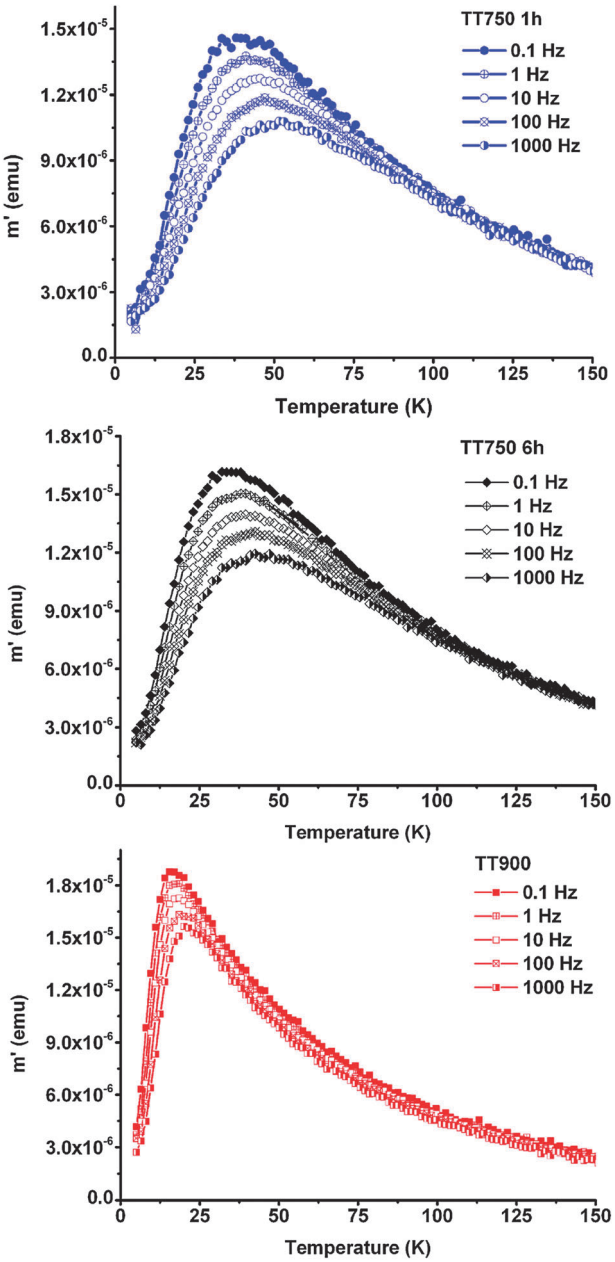

Fig. 9 Real component of the complex magnetization of the ZF750_1, ZF750_6 and ZF900_1 samples, respectively. In each graph the ZFC curves obtained for the different frequency of the external oscillating field are reported.

Taking into account the results obtained from the ac measurements and the equation reported above, the graphs shown in Fig. 10 were obtained for the three samples, where the linear fitting of the experimental points is also reported.

Following the Tronc model,[29] using the values of $<V>$ determined from the Scherrer equation applied to the XRD pattern of each sample, from the slope of each straight line a K_A value of 6.4×10^6, 1.2×10^6 and 1.5×10^5 (erg cm^{-3}) was determined for the ZF750_1, ZF750_6 and ZF900_1 samples, respectively. These results quantitatively confirm that the K_A value greatly decreases with the increase of temperature and

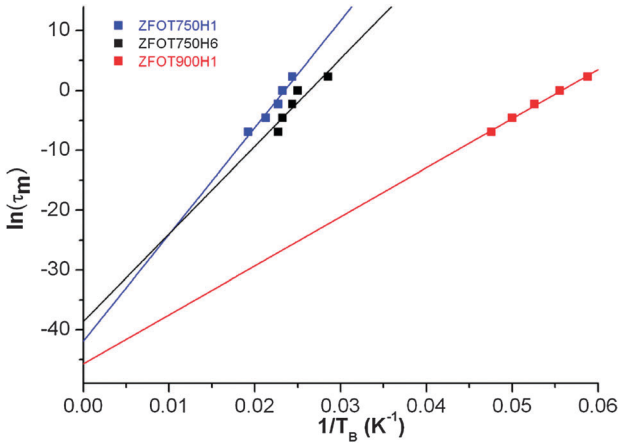

Fig. 10 ln τ_m *vs.* 1/TB as obtained from the real part of the ac ZFC curves. For each sample the linear fitting is also reported.

the duration of the thermal treatment, in agreement with the observed decrease of the blocking temperature observed in the static ZFC magnetization curves and in the Mössbauer spectroscopy measurements, and of the trend of the coercive field. Again, the anisotropy constant values are higher than those reported in ref. 14 for zinc ferrite nanoparticles of similar size, dispersed with higher loading in an amorphous silica matrix. Since it is possible to suppose that similar size corresponds to similar contribution of the surface anisotropy to the effective one, it is likely that the observed magnetic anisotropy increase is due to the high inversion degree of the zinc ferrite nanoparticles. The τ_0 values of 6.3×10^{-19}, 1.7×10^{-17} and 1.4×10^{-20} s were determined with the same fitting procedure for the ZF750_1, ZF750_6 and ZF900_1 sample, respectively. These values are much lower than those expected for ferrimagnetic nanoparticles, but they give a first clear indication of the presence of dipolar interaction among the particles, which are well-known to affect the pre-exponential factor[34] of the Arrhenius-like law.

In order to give a qualitative measurement of the strength of the dipolar interparticle interactions of each sample, magnetization measurements according to the TRM protocol were carried out in the temperature range of 5–400 K for all the samples. To this end, the samples were first cooled from 400 K to 5 K with an external static magnetic field of 25 Oe and then, after turning off the field, the magnetization was measured while warming up to 400 K. The magnetization measured with the TRM protocol decreases with the temperature increase, and when all the nanoparticles go to the superparamagnetic state, M_{TRM} falls to zero. From the TRM magnetization curves information about the distribution of magnetic anisotropy energy of the nanoparticles can be obtained, with no virtual contribution from the dipolar interparticle interactions. In fact, as reported in ref. 35 the derivative of the magnetization decay plot represents the distribution of anisotropy energy barriers with no magnetic environmental contribution due to the interactions. The TRM and the corresponding derivative curves are reported in Fig. 11.

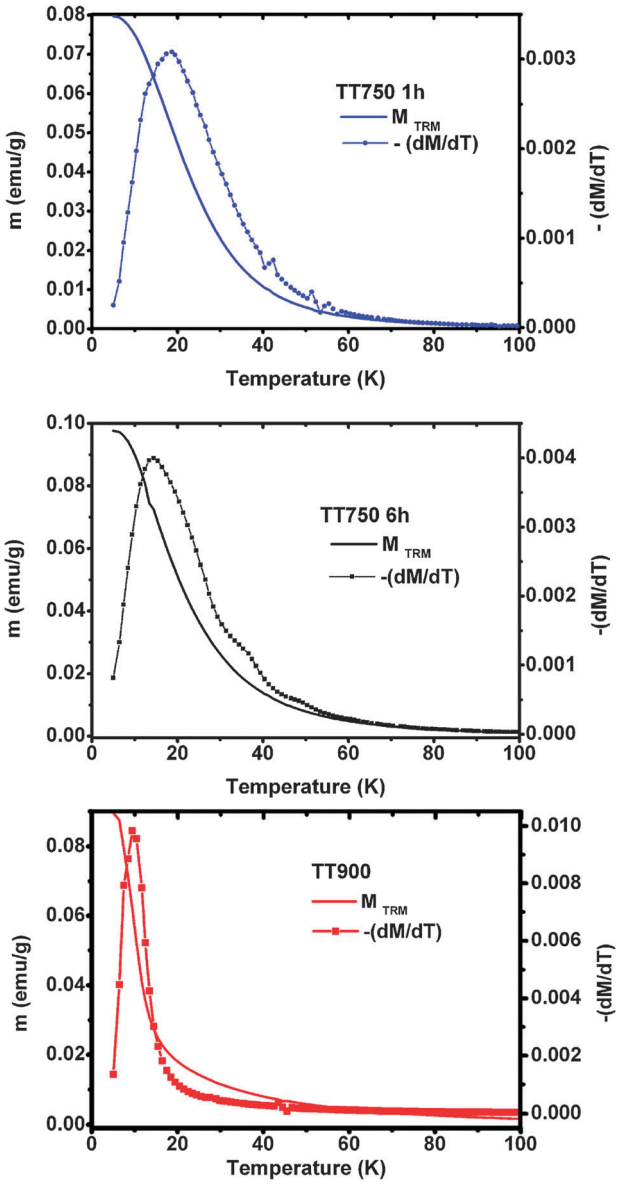

Fig. 11 TRM curves of samples ZF750_1, ZF750_6 and ZF900_1, respectively. The curves were obtained after cooling each sample in the same magnetic field used to measure the static ZFC–FC magnetizations, 25 Oe. Each graph shows also the opposite of the derivative of the TRM curves with respect to T, showing the distribution of anisotropy energy barriers with no magnetic environmental contribution due to the interparticle interactions.

As a consequence, the comparison of the T_{max} obtained from the static ZFC measurements with the temperature of the maximum of the TRM derivative curve can be considered as a qualitative measure of the strength of the interparticle magnetic interactions. The difference is 19 K for the ZF750_1 sample, 18 K for the ZF750_6 h sample, and 7 K for the ZF900_1 sample, indicating that the strength of the interactions is decreasing with the temperature and the duration of the thermal treatment. This fact is not easy to explain, as different contributions play here a non-independent role: even if one considers that the strength of magnetic dipolar interactions, the most probable interactions in our samples, increases with the magnetic moment of the interacting nanoparticles (proportional to their volume) and decreases with their separation distance, the role played by the different amount of precursor phases in each sample should also be taken into account together with the multiple effect of the variation of the inversion degree on the saturation magnetization of the zinc ferrite particles.

4. Conclusions

Static and dynamic magnetization measurements and Mössbauer spectroscopy were used to investigate the magnetic behavior of zinc ferrite nanocrystals dispersed on a highly porous silica aerogel. It was found by previous structural investigation that by varying the thermal treatment of the nanocomposite, the size of the $ZnFe_2O_4$ nanocrystals could be varied from 4 to 7 to 11 nm in samples ZF_750_1, ZF_750_6, ZF_900_1, and the inversion degree varied correspondingly from 0.4 to 0.3 to 0.2. These data are in line with what expected with increasing particle size, approaching the normal spinel structure of bulk zinc ferrite.

The nanocomposites are superparamagnetic at room temperature, with blocking temperatures of 37 K, 31 K, 15 K, as determined by ZFC–FC DC magnetization curves and 80 K, 75 K, 31 K, as determined by Mössbauer spectroscopy, and for the ZF_750_1, ZF_750_6, ZF_900_1 nanocomposites, respectively. In particular, these results point out that the superparamagnetic transition in the samples is dominated by the inversion degree rather than by the particle size, which would lead to an opposite effect on the blocking temperature. Moreover, the calculated effective magnetic anisotropy appears to be systematically higher than that measured for supported zinc ferrite nanoparticles of sizes similar to those of our samples, pointing out that this is due to their high inversion degree.

We acknowledge that the superparamagnetic behavior and in particular the blocking temperatures may also be affected by contributions arising from interparticle interactions in addition to those from the properties of the individual nanocrystals. In this work, the TRM protocol was used as a means to determine the blocking temperatures free from particle interactions. Comparison of the blocking temperatures determined by DC ZFC–FC magnetization curves and TRM data analysis provides a qualitative estimate of the strength of particle interactions in the samples. Based on these data, the contribution of particle interaction to the magnetic behavior of the nanocomposites is nearly the same in ZF_750_1 and ZF_750_6, and decreases significantly in ZF_900_1. These results could be tentatively ascribed, based on TEM investigation, to the occurrence of dipolar interactions which may decrease in sample ZF_900_1 due to the larger interparticle distance resulting from nanocrystal growth, despite the increase in the magnetization value.

The multitechnique magnetic investigation reported in this study enabled us to determine the value of the anisotropy constant K_A both by AC ZFC magnetization curves as well as by combined Mössbauer spectroscopy and DC magnetization.

The values obtained by both approaches give evidence that the anisotropy constant decreases from sample ZF_750_1 to ZF_750_6 to sample ZF_900_1, and are within the range expected for ferromagnetic nanoparticles.

Acknowledgements

The authors wish to thank the Italian Ministry for Education, University and Research (MIUR) through the PRIN 2009 call for financial support.

References

1 J. W. Verwey and E. L. Heilmann, *J. Chem. Phys.*, 1947, **15**, 174.
2 D. H. Han, H. L. Luo and Z. Yang, *J. Magn. Magn. Mater.*, 1996, **161**, 376.
3 Y. Tae-Jong, K. Jun Sung, K. Byung Geol, Y. Kyeong Nam, C. Myung-Haing and L. Jin-Kyu, *Angew. Chem., Int. Ed.*, 2005, **44**, 1068.
4 C. H. Cunningham, T. Arai, P. C. Yang, M. V. McConnell, J. M. Pauly and S. M. Connolly, *Magn. Reson. Med.*, 2005, **53**, 999.
5 K. Giri, K. Pellerin, W. Pongsaksawad, M. Sorescu and S. A. Majetich, *IEEE Trans. Magn.*, 2000, **36**, 3029.
6 D. S. Mathew and R.-S. Juang, *Chem. Eng. J.*, 2007, **129**, 51.
7 C. Yao, Q. Zeng, G. F. Goya, T. J. Torres, J. Liu, H. Wu, M. Ge, Y. Zeng, Y. Wang and J. Z. Jiang, *J. Phys. Chem. C*, 2007, **111**, 12274.
8 H. H. Hamdeh, J. C. Ho, S. A. Oliver, R. J. Willey, G. Oliveri and G. Busca, *J. Appl. Phys.*, 1997, **81**, 1851.
9 C. N. Chinnasamy, A. Narayanasamy, N. Ponpandian, K. Chattopadhyay, H. Guerault and J. M. Greneche, *J. Phys.: Condens. Matter*, 2000, **12**, 7795.
10 M. Hofmann, S. J. Campbell, H. Ehrhardt and R. Feyerherm, *J. Mater. Sci.*, 2004, **39**, 5057.
11 J. H. Shim, S. Lee, J. H. Park, S.-J. Han, Y. H. Jeong and Y. W. Cho, *Phys. Rev. B: Condens. Matter Mater. Phys.*, 2006, **73**, 064404.
12 M. K. Roy, B. Haldar and H. C. Verma, *Nanotechnology*, 2006, **17**, 232.
13 S. J. Stewart, S. J. A. Figueroa, J. M. Ramallo Lopez, S. G. Marchetti, J. F. Bengoa, R. J. Prado and F. G. Requejo, *Phys. Rev. B: Condens. Matter Mater. Phys.*, 2007, **75**, 073408.
14 V. Blanco-Gutierrez, M. J. Torralvo-Fernandez and R. Saez-Puche, *J. Phys. Chem. C*, 2010, **114**, 1789.
15 V. Blanco-Gutierrez, E. Climent-Pascual, M. J. Torralvo-Fernandez, R. Saez-Puche and M. T. Fernandez-Diaz, *J. Solid State Chem.*, 2011, **184**, 1608.
16 B. Antic, M. Perovic, A. Kremenovic, J. Blanusa, V. Spasojevic, P. Vulic, L. Bessais and E. S. Bozin, *J. Phys.: Condens. Matter*, 2013, **25**, 086001.
17 A. Sutka, R. Parna, M. Zamovskis, V. Kisand, G. Mezinskis, J. Kleperis, M. Maiorov and D. Jakovlev, *Phys. Status Solidi A*, 2013, 1.
18 D. Carta, C. Marras, D. Loche, G. Mountjoy, S. Ahmed and A. Corrias, *J. Chem. Phys.*, 2013, **138**, 054702.
19 M. F. Casula, D. Loche, S. Marras, G. Paschina and A. Corrias, *Langmuir*, 2007, **23**, 3509.
20 D. Loche, M. F. Casula, A. Falqui, S. Marras and A. Corrias, *J. Nanosci. Nanotechnol.*, 2010, **10**, 1008.
21 S. Brunauer, P. H. Emmet and E. Teller, *J. Am. Chem. Soc.*, 1938, **60**, 309.
22 P. Barret, L. G. Joyner and P. P. Halenda, *J. Am. Chem. Soc.*, 1951, **73**, 373.
23 F. Rouquerol, J. Rouquerol and K. S. W. Sing, *Adsorption by powders and porous solids: principles, methodology and applications*, Academic Press, London, 1999.
24 A. Lecloux and J. P. Pirard, *J. Colloid Interface Sci.*, 1979, **70**, 265.
25 P. Gütlich, R. Link and A. Trautwein, *Mössbauer spectroscopy and transition metal chemistry*, Springer-Verlag, Berlin, 1978.
26 Internal report DF-UCA/GC1-12.
27 M. Respaud, J. M. Broto, H. Rakoto, A. R. Fert, L. Thomas, B. Barbara, M. Verelst, E. Snoeck, P. Lecante, A. Mosset, J. Osuna, T. Ould Ely, C. Amiens and B. Chaudret, *Phys. Rev. B: Condens. Matter Mater. Phys.*, 1998, **57**, 2925.
28 L. Neel, *Ann. Geophys.*, 1949, **5**, 99.
29 E. Tronc, P. Prene, J. P. Jolivet, F. d'Orazio, F. Lucari, D. Fiorani, M. Godinho, R. Cherkaoui, M. Nogues and J. L. Dorman, *Hyperfine Interact.*, 1995, **95**, 129.
30 C. Cannas, G. Concas, D. Gatteschi, A. Falqui, A. Musinu, G. Piccaluga, C. Sangregorio and G. Spano, *Phys. Chem. Chem. Phys.*, 2001, **3**, 832.
31 A. Pradeep, P. Pryadharsini and G. Chandrasekaran, *J. Alloys Compd.*, 2011, **509**, 3917.
32 L. D. Tung, V. Kolesnichenko, G. Caruntu, D. Caruntu, Y. Remond, V. O. Golub, C. J. O'Connor and L. Spinu, *Phys. Rev. B: Condens. Matter Mater. Phys.*, 2002, **319**, 116.
33 C. N. Chinnasamy, A. Narayanasamy, N. Ponpandian, K. Chattopadhyay, H. Guerault and J. M. Greneche, *Scr. Mater.*, 2001, **44**, 1407.
34 J. L. Dormann, F. D'Orazio, F. Lucari, E. Tronc, P. Prené, J. P. Jolivet, D. Fiorani, R. Cherkaoui and M. Noguès, *Phys. Rev. B: Condens. Matter Mater. Phys.*, 1996, **53**, 14291.
35 J. Rondinone, A. C. S. Samia and Z. J. Zhang, *J. Phys. Chem. B*, 1999, **103**, 6876.

